90-04515/

CANADA

DEPARTMENT OF ENERGY, MINES AND RESOURCES

MINES BRANCH

OTTAWA

PHYSICAL METALLURGY DIVISION

INTERNAL REPORT PM-R-71-6

A STUDY OF THE PROPERTIES AND SINTERING BEHAVIOUR OF CERTAIN NICKEL POWDERS

PROGRESS REPORT No. 3

by

H. M. Skelly and C. F. Dixon

Nuclear and Powder Metallurgy Section

April 30, 1971

PHYSICAL METALLURGY DIVISION

INTERNAL REPORT PM-R-71-6

A STUDY OF THE PROPERTIES AND SINTERING BEHAVIOUR OF CERTAIN NICKEL POWDERS

PROGRESS REPORT No. 3

by

H. M. Skelly* and C. F. Dixon**

- - - - -

ABSTRACT

Four nickel powders of differing morphology and particle size were examined and tested in the uncompacted and compacted conditions. The effect of blending three of the powders was also studied.

Particle shape and size were found to have a significant effect on powder behaviour.

---

* Research Scientist and ** Scientific Officer, Nuclear and Powder Metallurgy Section, Physical Metallurgy Division, Mines Branch, Department of Energy, Mines and Resources, Ottawa, Canada.

CONTENTS

		Page
	Abstract	i
1.	Introduction	1
2.	Test Material	1
3.	Experimental Procedure	2
	3.1 Testing of Powders and Blends	2
	3.2 Preparation and Testing of Green Compacts	2
	3.3 Microexamination of Green Compacts	3
4.	Results and Discussion	3
	4.1 Properties of Powders and Blends	3
	4.2 Properties of Green Compacts	4
	4.2.1 Density and Porosity	4
	4.2.2 Transverse Rupture Strength	5
	4.2.3 Microstructure	5
5.	Conclusions	6
6.	Acknowledgements	6
7.	References	6
	Figures 1 - 18	9 - 22

- - - -

1. INTRODUCTION

The work described in this report is a continuation of a study of the effect of powder properties on the compacting and sintering behaviour of nickel powders [1,2].

2. TEST MATERIAL

The following four nickel powders were investigated:

Powder Grade	Morphology	Particle Size	
		U.S. Sieve No.	Microns
S	Spheroidal, pebbly	+100 to -325 mesh*	>149 to <44
-100+140S	" "	-100 to +140 mesh	<149 to >105
SF 300	" "	-325 mesh	~19
G-29	Loose, dendritic agglomerates	-325 mesh	~6

*Sherritt Gordon S grade, which is a natural blend of size fractions, gave the following screen analysis:

U.S. Sieve No:	+80	-80 +100	-100 +140	-140 +200	-200 +230	-230 +325	-325
Wt.% retained:	0.3	0.9	18.6	28.4	16.4	20.6	14.8

SF300 is produced by a combination of process variation and screening which gives a narrow range of fine particles, similar in appearance to the S grade particles. The -100 + 140S grade is a screened fraction of the standard S product. These three grades are all characterized by dense, spheroidal particles with a pebbly surface. The G-29 grade is intentionally produced as a low-density powder with a high specific surface area and a fine particle size. Further details of the powders' properties are given in the initial progress report [1].

Besides these four powders, six blends of the following compositions (prepared in a twin-shell laboratory blender) were also investigated: SF300 with 25%, 50% and 75% G-29, and -100 + 140S with the same percentages of G-29.

3. EXPERIMENTAL PROCEDURE

3.1 Testing of Powders and Blends

Flow rate was determined as described in Metal Powder Industries Federation (MPIF) Standard 3-45 in which the time taken for 50g of powder to flow through the orifice in a standardized funnel is measured. Apparent density was obtained by calculation from the weight of powder required to fill a container of known volume, as in MPIF Standard 28-59.

A "Tap-Pak Volumeter" was used to determine the tap density. The volume of a known weight of powder sample is measured after a given number of "taps" (75 in this case) in a calibrated cylinder. It was found that continuing the tapping beyond 75 taps produced no significant change in the volume of the powder. The ratio of sample weight to volume after tapping gives the tap density.

The compression ratio was determined for a range of compacting pressures by calculating the ratio of the height of powder in the die before and after compaction.

3.2 Preparation and Testing of Green Compacts

Using a 100-ton hydraulic press, transverse rupture test specimens for determination of green strength were prepared in a die with cavity dimensions of 1-1/4-in. by 1/2-in.; the test specimens were about 1/4-in. thick. No lubricant was mixed in with the powders or blends, but the die itself was lubricated with stearic acid.

Mechanical testing was carried out on an Instron machine, using the procedure described in MPIF Standard 15-62 except that the rate of loading was 200 lb/min instead of 20 lb/min. In this test, the specimen is supported at each end and broken by applying a load at the centre. Green strength is calculated from the formula:

$$S = \frac{3 \times P \times L}{2 \times t^2 \times w}$$

where
- S = green strength (psi)
- P = load in lb required to rupture
- L = distance between supports (1 in.)
- w = width of specimen (in.)
- t = thickness of specimen (in.)

The transverse rupture test specimens were also used to determine the density and porosity of green compacts. Density was determined by weighing the compact in air and calculating the volume from its dimensions (MPIF Standard 13-62); porosity was calculated from theoretical and actual densities.

3.3 Microexamination of Green Compacts

Several transverse rupture specimens were mounted and polished for microexamination. Fractured surfaces of the same specimens were also examined by the scanning electron microscope.

4. RESULTS AND DISCUSSION

4.1 Properties of Powders and Blends

The flow rates of the four powders, given in an earlier report [1], were as follows:

S:	17.9 sec/50 g
-100+140S:	18.7 sec/50 g
SF300:	20.6 sec/50 g
G-29:	no flow

All but one of the six blends gave a "no flow" result. The exception was -100+140S with 25% G-29, which had a flow rate of 18.6 sec/50 g. The irregular shape and fine size of the G-29 particles cause the powder to agglomerate, and this results in poor flowability as the orifice of the flow rate funnel becomes clogged.

The apparent and tap densities of the powders and blends are listed in Table 1. The apparent densities of the four powders have been reported before [1] but are included here for completeness. Also given in Table 1 is the ratio of tap density to apparent density.

The apparent densities of the blends decrease with increasing content of G-29. Tap densities follow the same trends as apparent densities.

The ratio of tap density to apparent density might be considered as the compression ratio for zero compaction pressure. Hausner [3] has suggested that this ratio is related to friction conditions existing between the powder particles. If this is the case, interparticle friction is least in -100+140S and greatest in G-29. Also, addition of G-29 to -100+140S and to SF300 increases the interparticle friction. This is consistent with the fact that surface area and texture are important factors influencing interparticle friction, as the G-29 particles are finer with a different texture compared to S particles.

The compression ratios of all powders and blends for compacting pressures ranging from 42.7 to 128 ksi are listed in Table 2. Plots of compression ratio against compacting pressure for the powders and blends are shown in Figures 1 to 3. The plots for the four powders (Figure 1) show that, while S and -100+140S are closely similar, SF300, (i.e., the fine fraction) is more compressible, and G-29 is more compressible than SF300. The plots for the blends of G-29 with -100+140S and SF300 (Figures 2 and 3, respectively) show little change with additions of 25% G-29 but, as the G-29 content is increased, the compression ratio increases.

Comparison of the values for apparent density (Table 1) with the compression ratios (Table 2) show that as the apparent density of the powders and blends increases, the compression ratio decreases.

4.2 Properties of Green Compacts

4.2.1 Density and Porosity

Table 3 lists the densities of the green compacts, and in Figure 4 densities for the four powders are plotted against the compacting pressures. The densities in Figure 4 are also expressed as a percentage of theoretical density (TD) for nickel (8.90 g/cc). The values given for zero compacting pressure are the apparent densities of the powders. These plots show that there is no significant difference between the densities of S and -100+140S samples for the range of compacting pressures investigated. The plots for SF300 and G-29 compacts are similar except for a slight divergence at low and high compacting pressures. The densities of the latter compacts are below those of S and -100+140S except for SF300 compacted at 96 ksi which then increases to the value for S and -100+140S.

The relationship between green density and blend composition for the two blends is shown by the plots in Figures 5 and 6, which also show density expressed as a percentage of theoretical density (TD). Besides the three compacting pressures, values are plotted for zero compaction (apparent and tap densities). It can be seen that in the case of blends of -100+140S with G-29 (Figure 5), maximum density for all plots occurs at 25% G-29. Figure 6 shows that blending SF300 with G-29 has little effect on density for all levels of compaction.

Values for total porosity, calculated from green density, are listed in Table 4. Minimum porosity, 17.8%, occurred with -100+140S blended with 25% G-29 and compacted at 96 ksi, and maximum porosity, 42.0%, occurred with SF300 compacted at 42.7 ksi.

4.2.2 Transverse Rupture Strength

Values of transverse rupture strength for four compacting pressures are listed in Table 5 and plotted in Figures 7 to 9.

In Figure 7 the transverse rupture strength of the four powders is plotted against compacting pressure. The powders, in order of increasing strength are -100+140S, S, G-29 and SF300 at all compacting pressures. At the low compacting pressure of 42.6 ksi the range of green strengths is small, but it increases with increasing compacting pressure and is quite large at 128 ksi.

The relationship between transverse rupture strength, blend composition and compacting pressure is shown by the plots in Figures 8 and 9. Figure 8 shows an increase in green strength at all compacting pressures as the percentage of G-29 increases in blends with -100+140S. This increase becomes more marked as the compacting pressure increases. Figure 9 shows that at the low compacting pressure (42.7 ksi), blending G-29 with SF300 has little or no effect on transverse rupture strength, but at the higher compacting pressures addition of 25% G-29 results in a marked drop in green strength, which is then little changed as the G-29 content increases.

The transverse rupture strength is not necessarily directly proportional to green density. For the four compacting pressures used, highest strength was obtained with SF300 although it had the lowest density at 42.7 ksi and at 64 ksi and did not have the highest density at 96 ksi (Table 3). This indicates that, where green strength is concerned, binding between particles is more important than mere filling-in of voids.

4.2.3 Microstructure

The microstructure of -100+140S blended with 25% G-29 and compacted at 64 ksi is shown in Figures 10 and 11. The fine particles of G-29 can be seen interspersed between the larger -100+140S particles. There is also evidence of interparticle welding.

Figures 12 and 13 are photomicrographs of -100+140S compacted at 96 ksi. Greater deformation of the particles is evident as compared with Figures 10 and 11. Again, there is indication of interparticle welding.

Figures 14 to 18 are scanning electron micrographs of the fractured surface of the specimens whose microstructure is shown in Figures 10 to 13. Several other specimens were examined by scanning electron microscope but none of them exhibited obvious signs of interparticle welding. This might be because the bond between welded particles, being the strongest, does not give way during fracture, which will occur preferentially between the weaker, mechanical bonds. There is a suggestion of welding between two

particles at the centre of Figure 16, which illustrates details of the surfaces of deformed particles.

5. CONCLUSIONS

1. The flow rate of rough, spheroidal particles, coarse (<149 to >105μ) or fine (~ 19μ), is reduced by blending them with fine (~ 6μ), dendritic, agglomerated particles.

2. The apparent and tap densities of rough, spheroidal particles, coarse (<149 to >105μ) or fine (~19μ), decrease with increasing blended additions of fine (~ 6μ), dendritic, agglomerated particles.

3. Optimum packing between rough, spheroidal particles (<149 to >105μ) and fine (~ 6μ), dendritic, agglomerated particles occurs at about 25% content of the latter for all compacting pressures from 0 to 96 ksi.

4. Blending of fine (~ 6μ), dendritic, agglomerated particles with rough, spheroidal particles (~ 19μ) has no significant effect on density at all compacting pressures from 0 to 96 ksi.

5. There is evidence of cold-welding between particles during compaction.

6. High green density does not necessarily result in high green strength.

6. ACKNOWLEDGEMENTS

Most of the laboratory work was performed by Mr. J. McGoey, Technical Assistant in this Section.

The scanning electron micrographs were prepared by Dr. K. M. Pickwick of the Metal Physics Section.

7. REFERENCES

1. H. M. Skelly and C. F. Dixon, "A Study of the Properties and Sintering Behaviour of Certain Nickel Powders", Progress Report No. 1, PMD Internal Report PM-R-68-9, Mines Branch, Dept. of Energy, Mines and Resources, Ottawa (Apr. 23, 1968).

2. H. M. Skelly and C. F. Dixon, "A Study of the Properties and Sintering Behaviour of Certain Nickel Powders", Progress Report No. 2, PMD Internal Report PM-R-68-18, Mines Branch, Department of Energy, Mines and Resources, Ottawa (Nov. 5, 1968).

3. Henry H. Hausner, "Friction Conditions in a Mass of Metal Powder", Int. J. Powder Metallurgy, 3, No. 4, 7-13 (1967).

HMS/CFD/gm

TABLE 1

Apparent and Tap Densities of Powders and Blends

Sample	AD* (g/cc)	TD* 75 taps (g/cc)	TD/AD
S	4.36**	5.05	1.16
-100+140S	4.38**	4.90	1.12
SF300	3.48**	4.10	1.18
G-29	3.06**	4.03	1.32
-100+140S with 25% G-29	4.90	5.68	1.16
" " " 50% G-29	4.39	5.43	1.24
" " " 75% G-29	3.70	4.63	1.25
SF300 with 25% G-29	3.64	4.54	1.25
" " 50% G-29	3.54	4.50	1.27
" " 75% G-29	3.33	4.20	1.26

*AD = apparent density TD = tap density
** taken from reference no. 1

TABLE 2

Compression Ratios of Powders and Blends

Compacting Pressure (ksi)	Compression Ratio									
					-100+140S with:			SF300 with:		
	S	-100 +140 S	SF300	G-29	25% G-29	50% G-29	75% G-29	25% G-29	50% G-29	75% G-29
42.7	1.30	1.26	1.45	1.90	1.32	1.51	1.69	1.57	1.62	1.80
53.3	1.40	1.38	1.62	1.94	1.37	1.51	1.79	1.65	1.73	1.87
64	1.44	1.43	1.69	2.04	1.43	1.54	1.77	1.71	1.84	1.87
66.7	1.45	1.43	1.72	2.07	1.44	1.51	1.85	1.82	1.84	1.97
80	1.50	1.52	1.79	2.14	1.46	1.59	1.85	1.89	1.92	1.99
96	1.47	1.56	1.88	2.26	1.53	1.65	1.92	1.87	1.95	2.03
128	1.68	1.65	1.94	2.42	1.58	1.74	2.06	1.97	2.06	2.18

TABLE 3

Density of Green Compacts

Compacting Pressure (ksi)	Density (g/cc)									
					-100+140S with:			SF300 with:		
	S	-100 +140 S	SF300	G-29	25% G-29	50% G-29	75% G-29	25% G-29	50% G-29	75% G-29
42.7	5.60	5.56	5.16	5.36	6.51	6.28	5.75	5.60	5.45	5.56
64	6.41	6.32	6.00	6.06	7.14	6.61	6.33	6.26	6.22	6.17
96	7.01	7.06	7.02	6.54	7.31	7.10	6.78	6.79	6.75	6.65

TABLE 4

Porosity of Green Compacts

Compacting Pressure (ksi)	Porosity (%)									
					-100+140S with:			SF300 with:		
	S	-100 +140 S	SF300	G-29	25% G-29	50% G-29	75% G-29	25% G-29	50% G-29	75% G-29
42.7	37.0	37.5	42.0	39.7	26.9	29.5	35.3	37.1	38.8	35.6
64	28.0	29.0	32.6	32.0	19.8	25.7	28.9	29.7	30.1	30.6
96	21.2	20.7	21.1	26.5	17.8	20.2	23.8	23.7	24.1	25.3

TABLE 5

Transverse Rupture Strength of Green Compacts

Compacting Pressure (ksi)	Transverse Rupture Strength (psi)									
					-100+140S with:			SF300 with:		
	S	-100 +140 S	SF300	G-29	25% G-29	50% G-29	75% G-29	25% G-29	50% G-29	75% G-29
42.7	51	31	239	162	53	70	80	152	145	150
64.0	357	252	838	546	192	285	361	462	571	600
96.0	766	514	1915	1160	529	623	816	1036	1161	1285
128.0	845	741	2443	1488	856	945	1095	1667	1805	1492

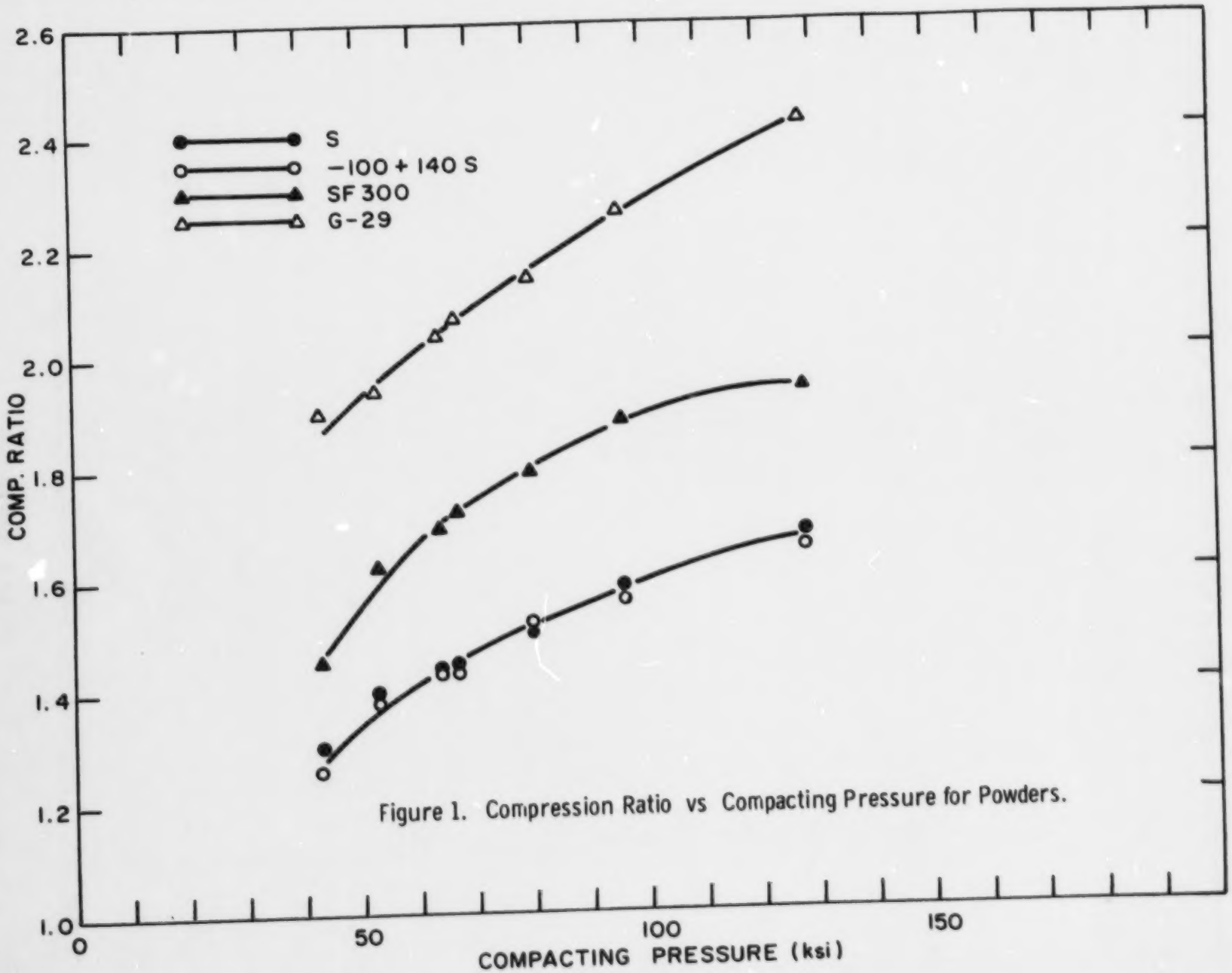

Figure 1. Compression Ratio vs Compacting Pressure for Powders.

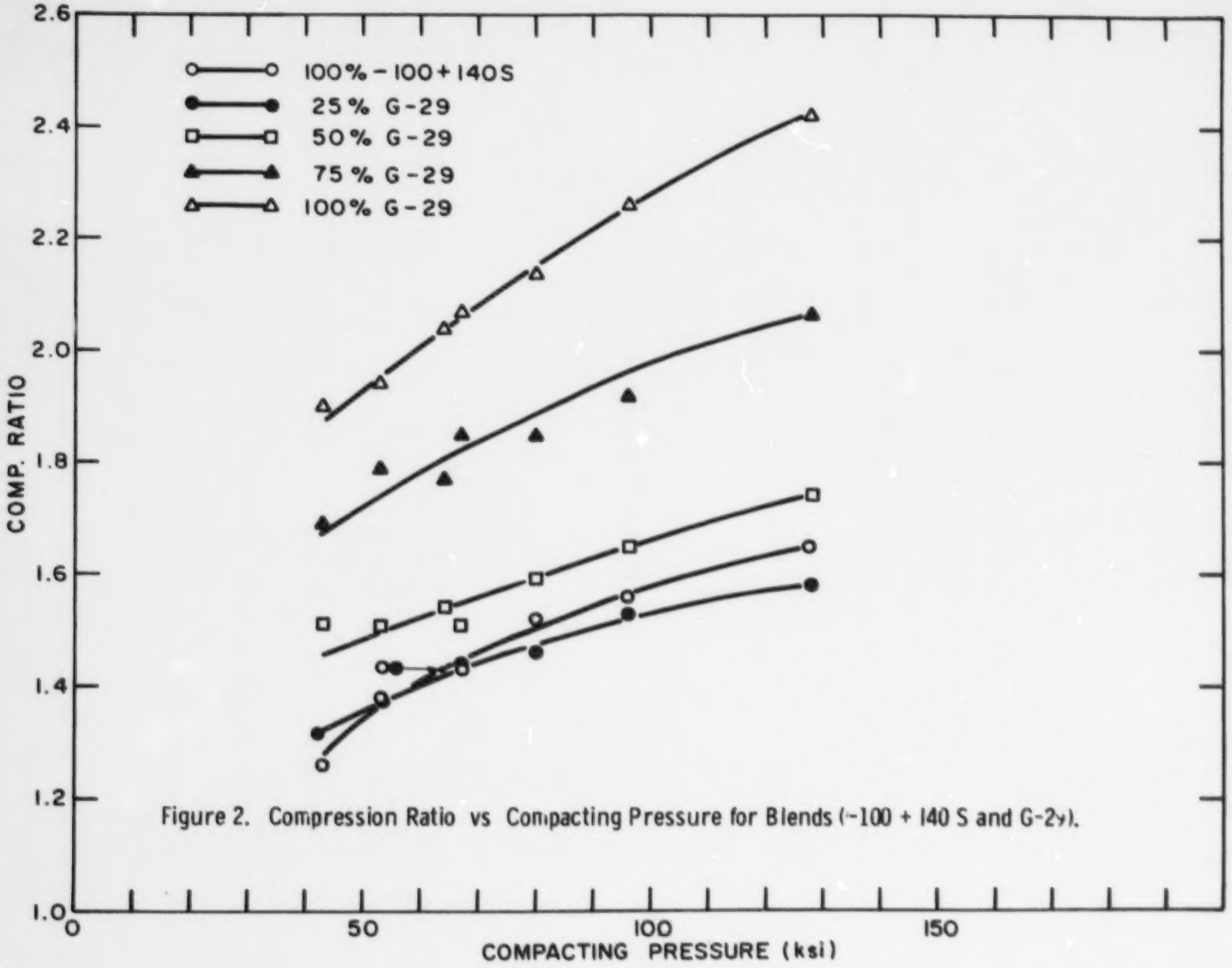

Figure 2. Compression Ratio vs Compacting Pressure for Blends (-100 + 140 S and G-29).

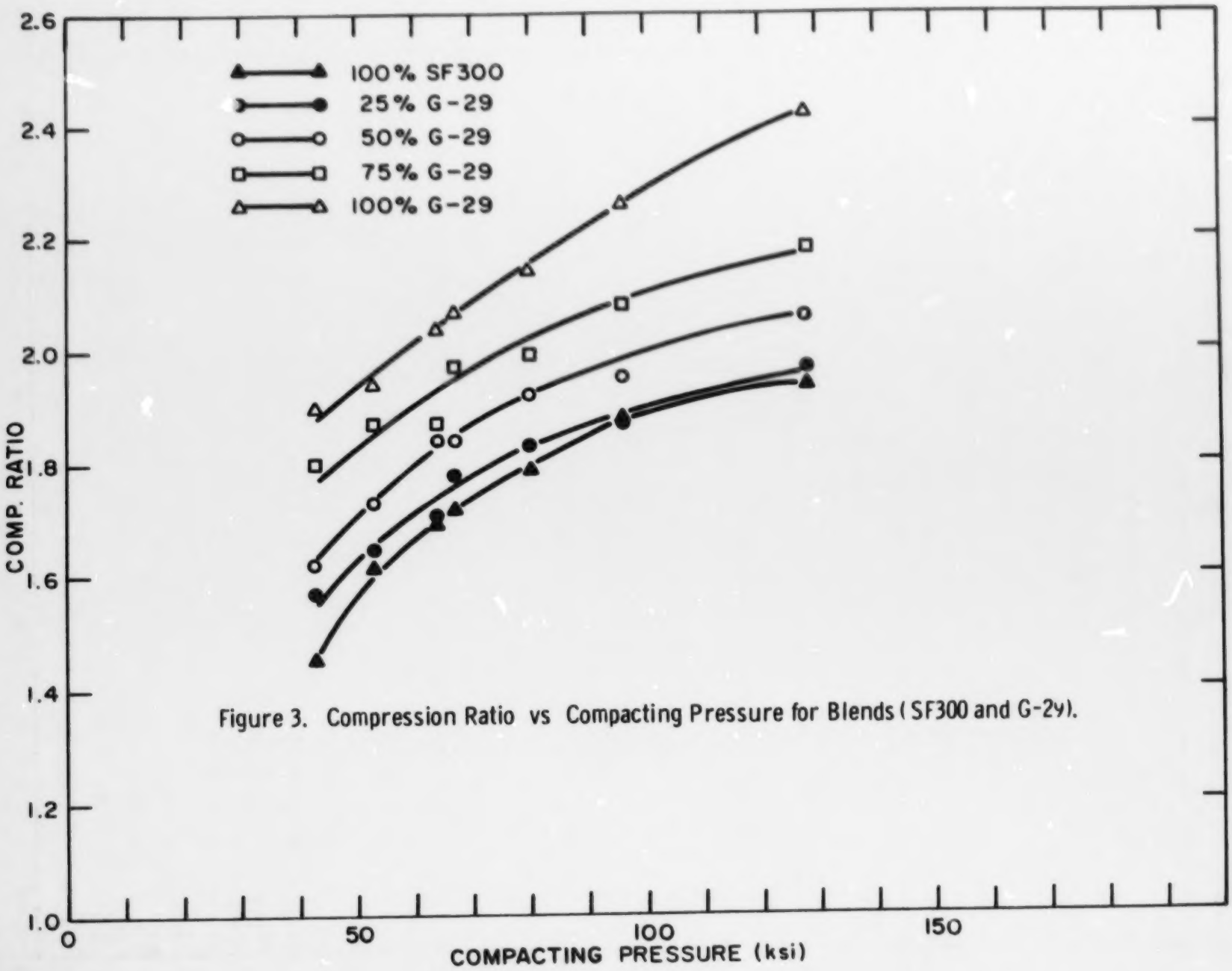

Figure 3. Compression Ratio vs Compacting Pressure for Blends (SF300 and G-29).

Figure 4. Green Density vs Compacting Pressure for Powders

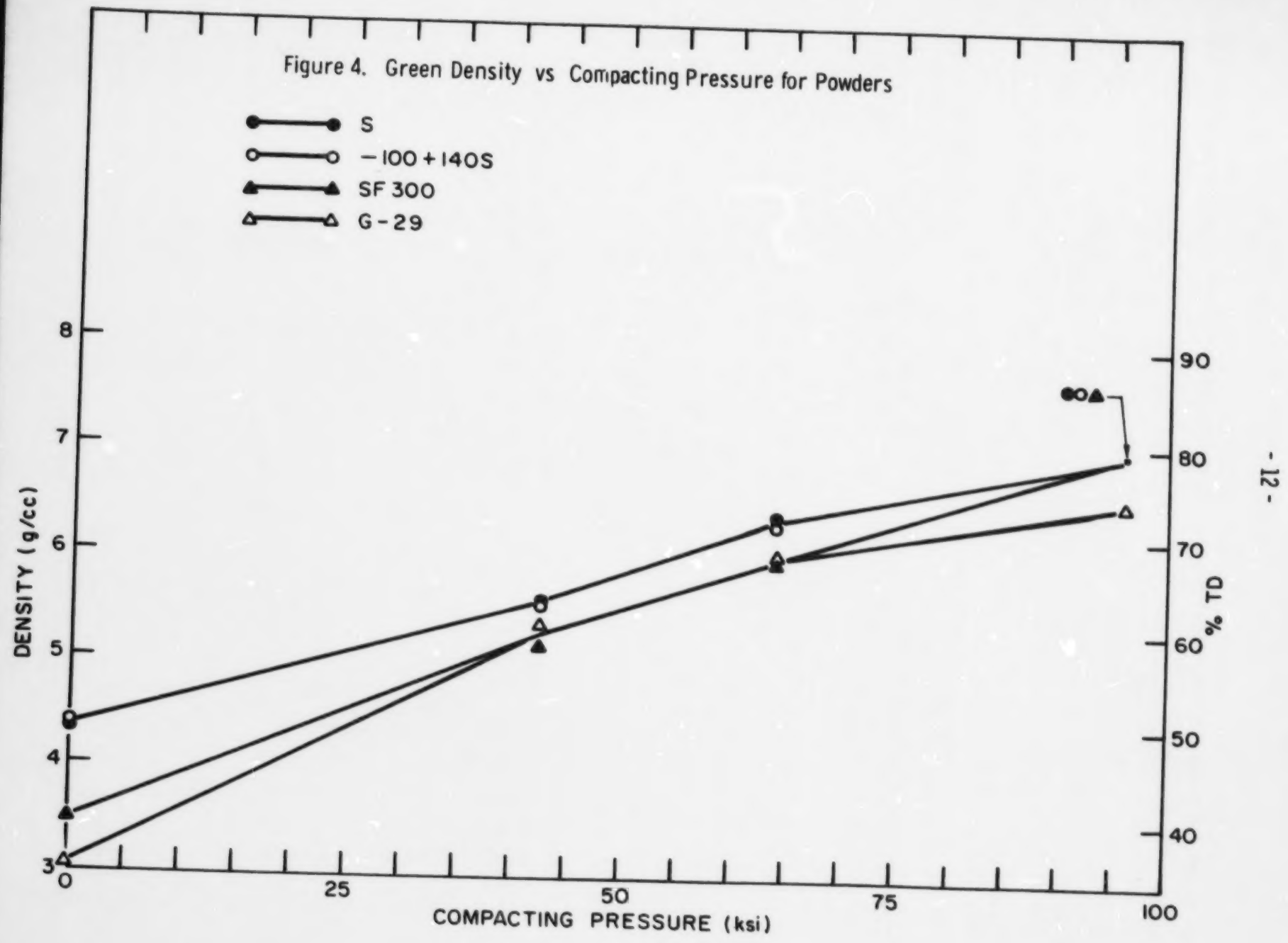

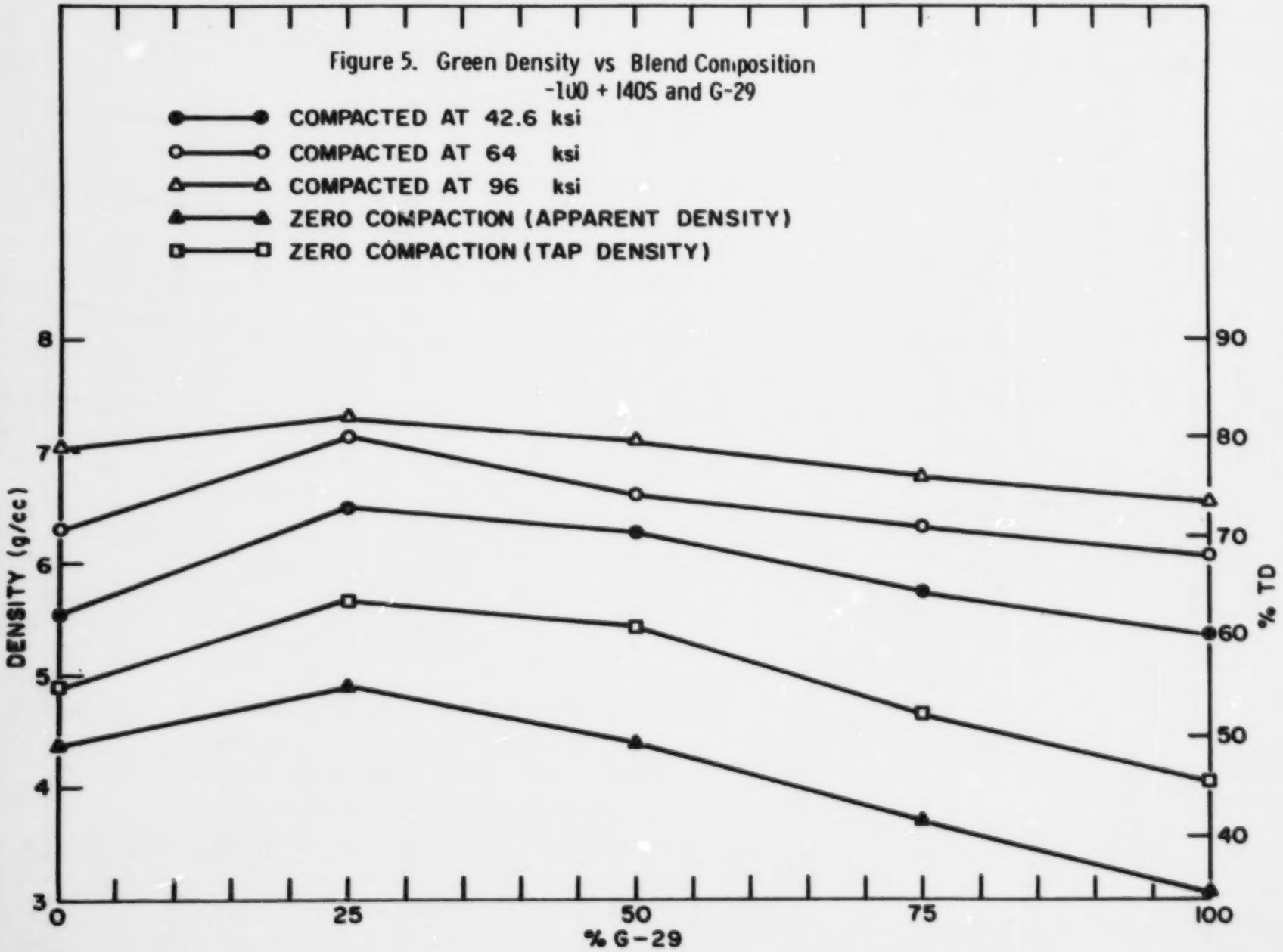

Figure 5. Green Density vs Blend Composition
-100 + 140S and G-29

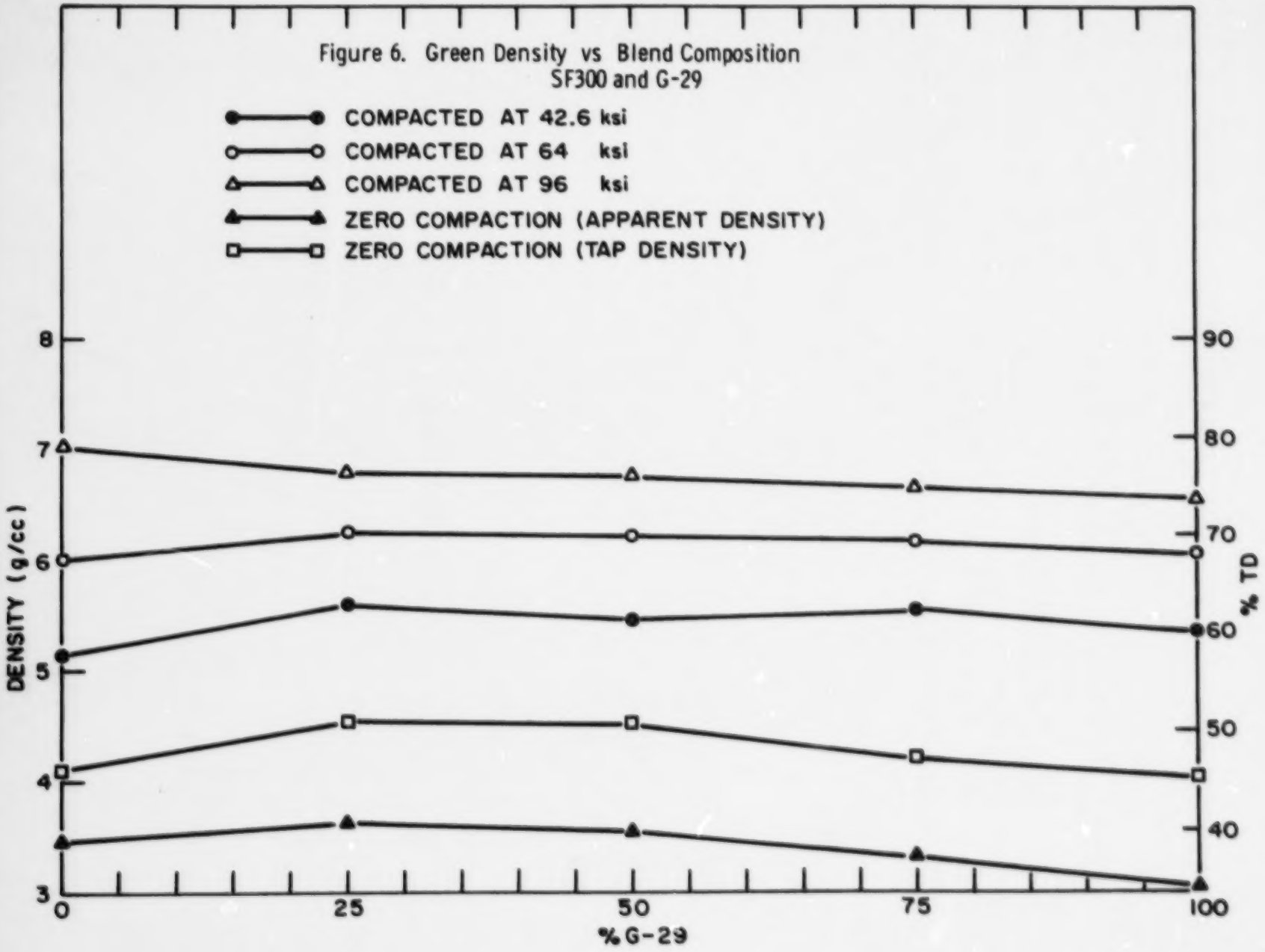

Figure 6. Green Density vs Blend Composition
SF300 and G-29

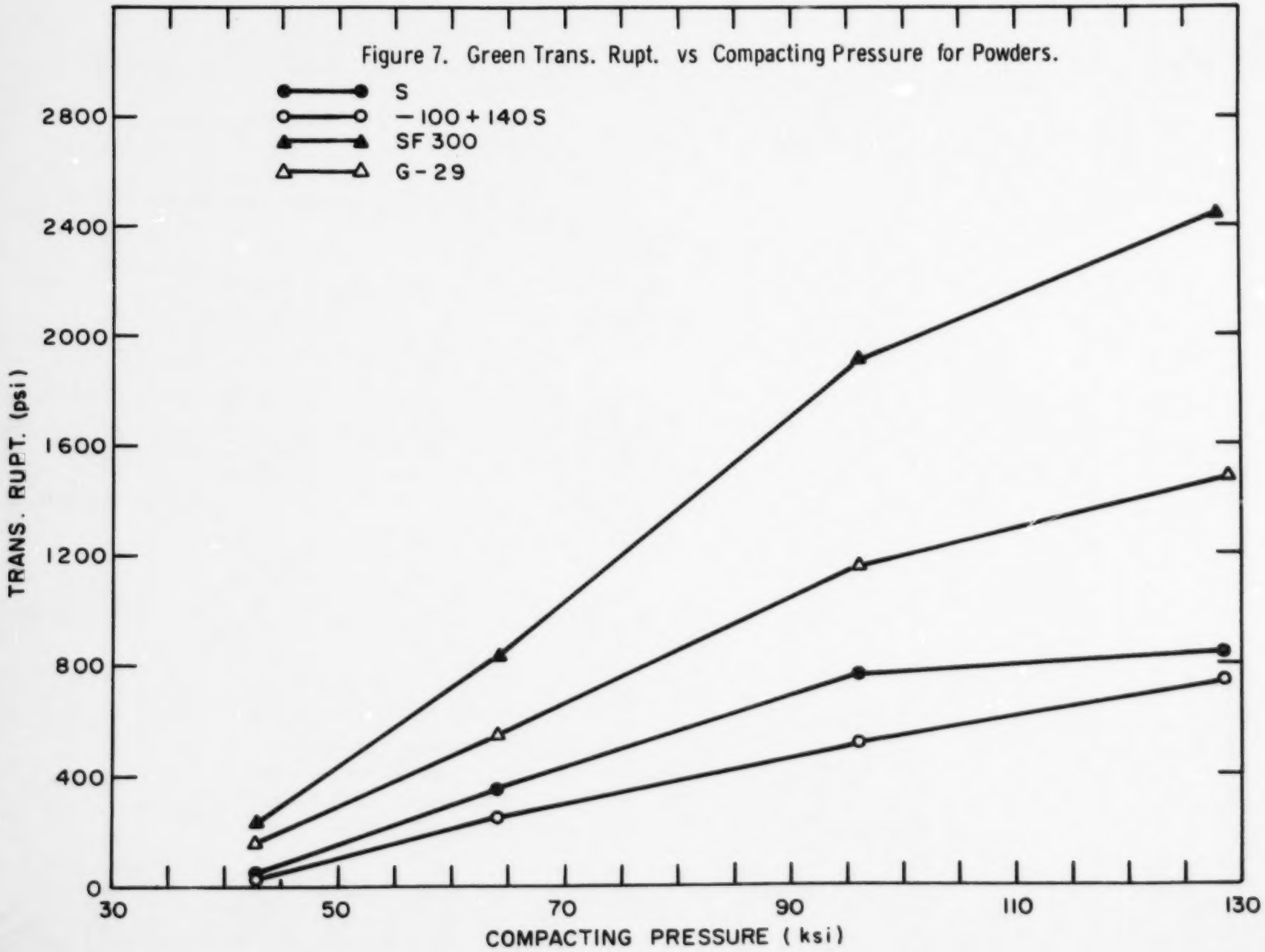

Figure 7. Green Trans. Rupt. vs Compacting Pressure for Powders.

Figure 8. Green Trans. Rupt. vs Blend Composition (-100 +140 S and G-29).

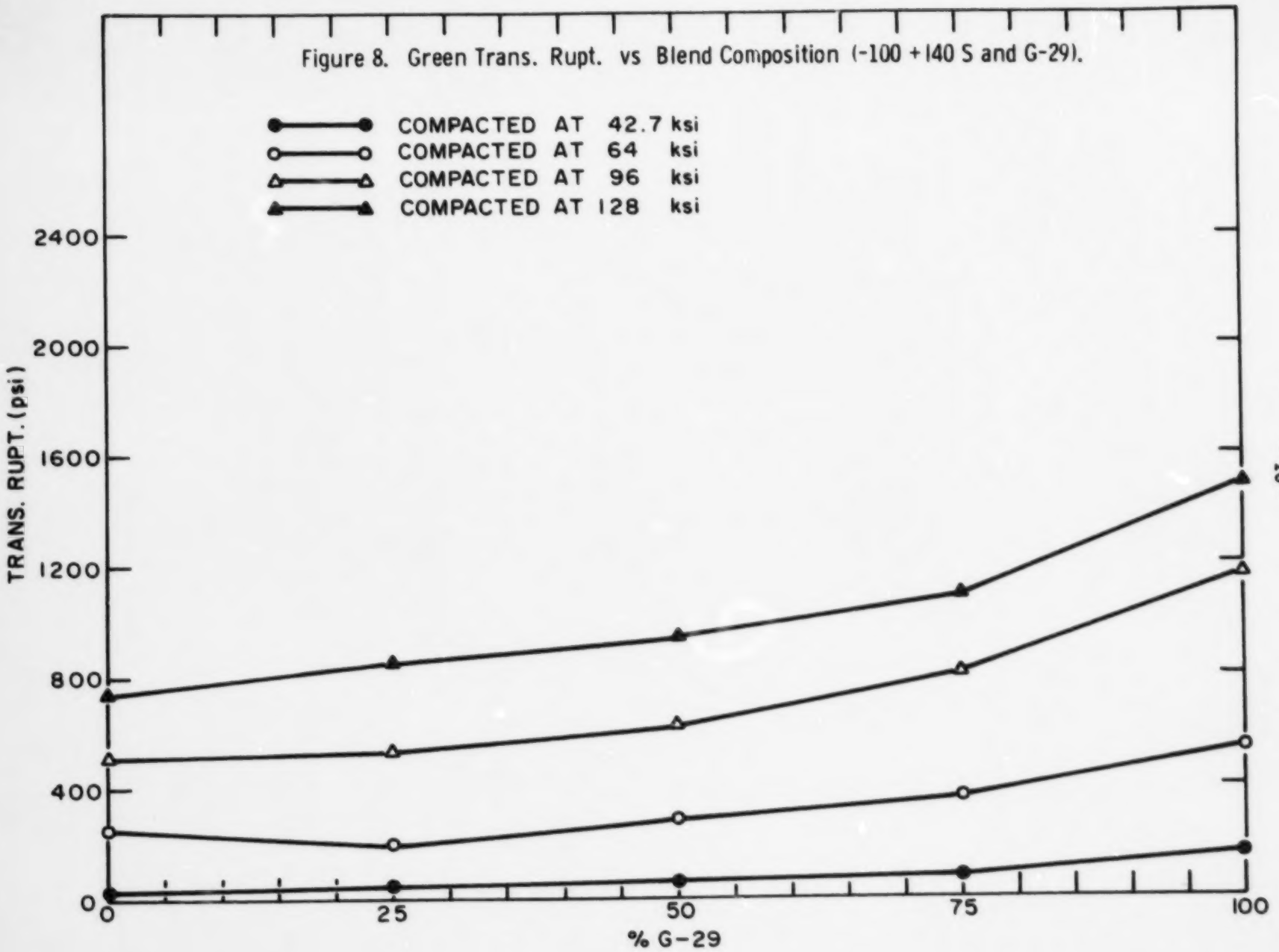

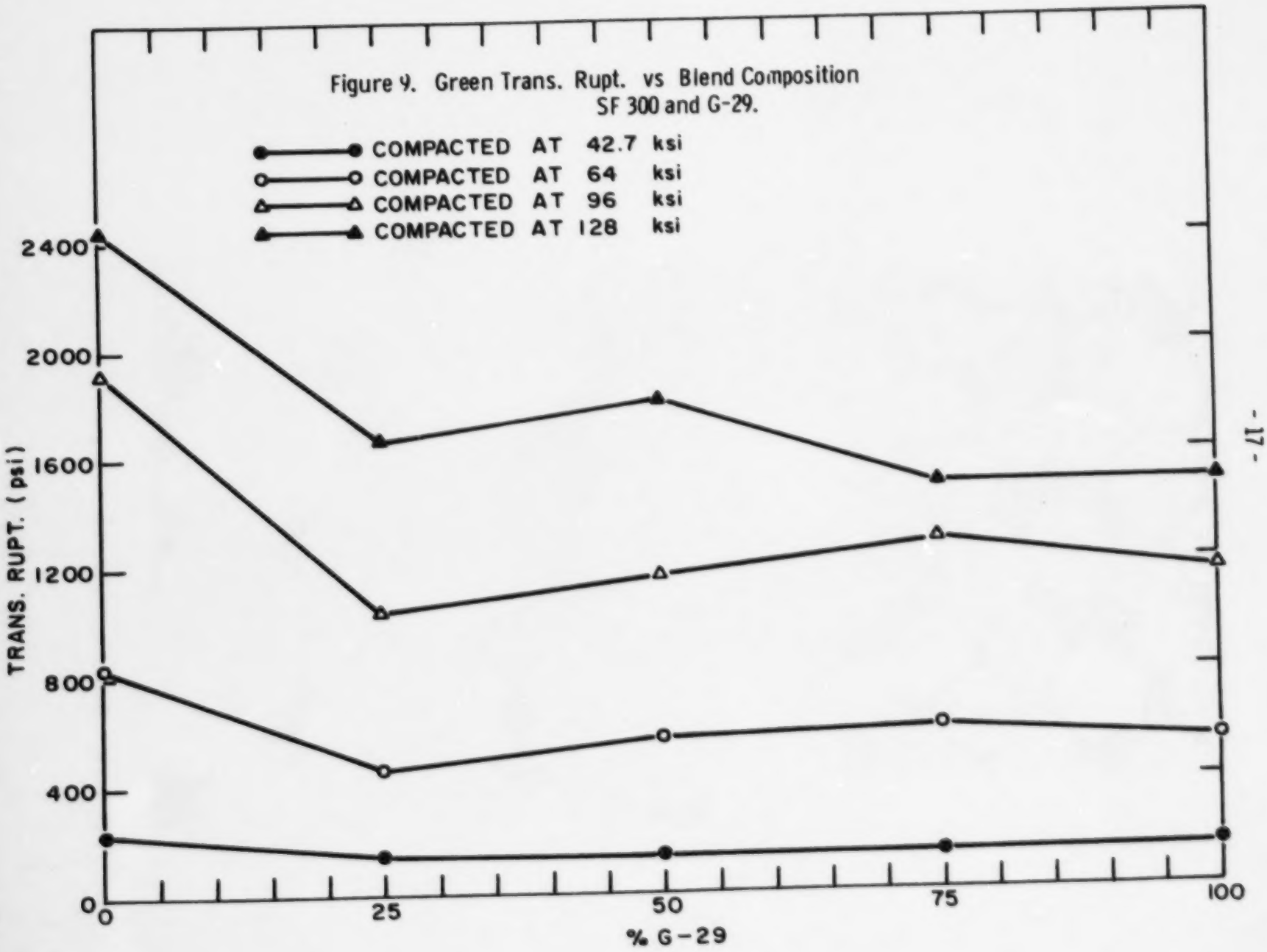

Figure 9. Green Trans. Rupt. vs Blend Composition SF 300 and G-29.

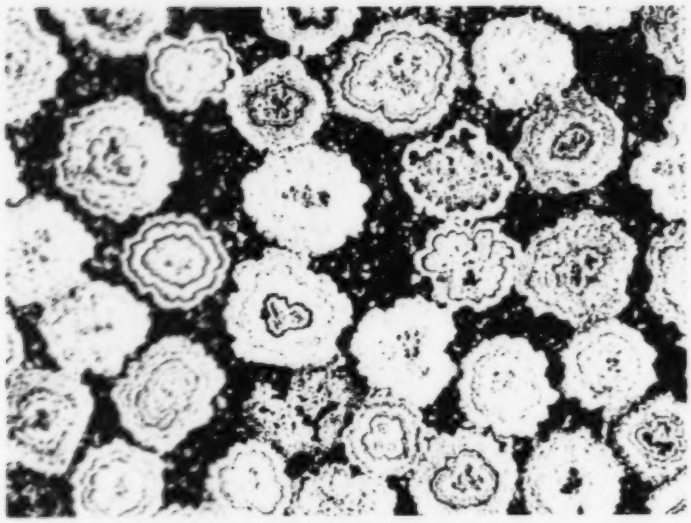

Etched X150

Figure 10. Microstructure -100+140S blended with 25% G-29. Compacted at 64 ksi.

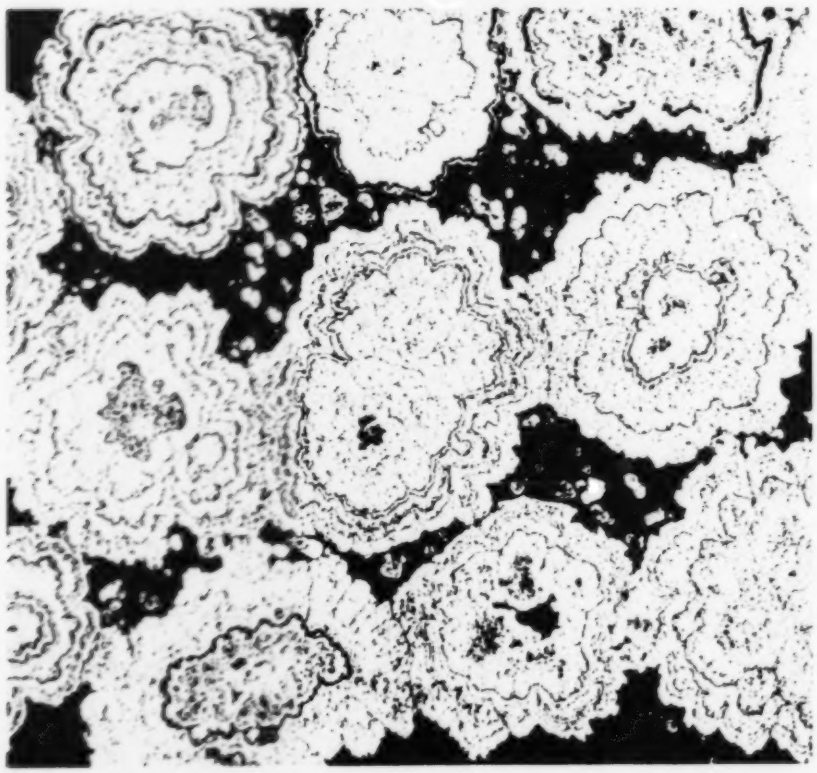

Etched X400

Figure 11. Same as Figure 10, at higher magnification.

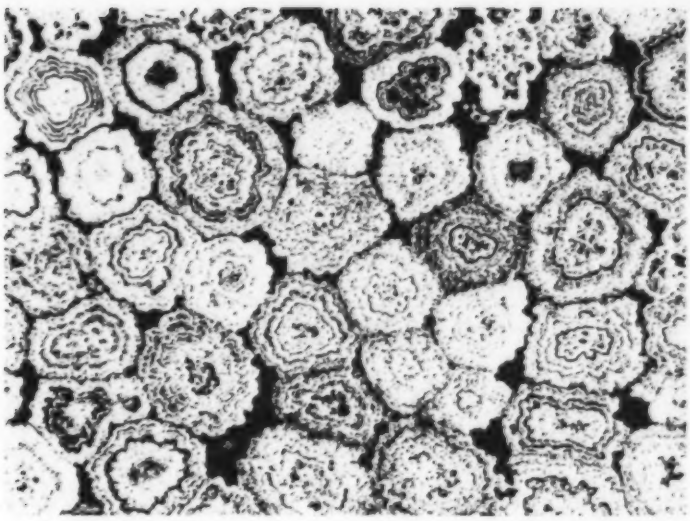

Etched X150

Figure 12. Microstructure of -100+140S compacted at 96 ksi.

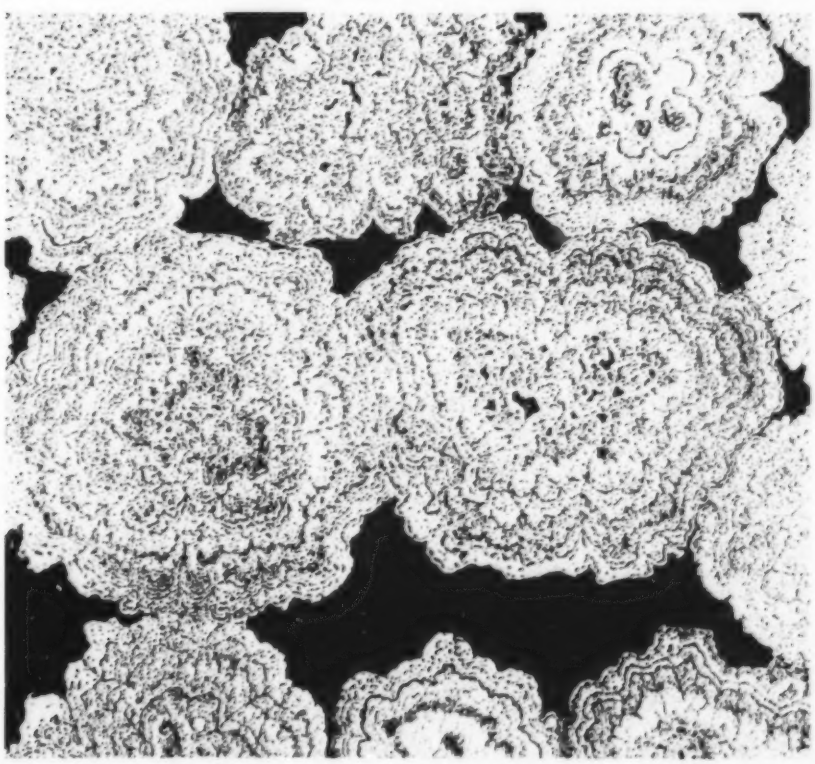

Etched X400

Figure 13. Same as Figure 12, at higher magnification.
(Etchant for Figures 10 to 13: Carapella's Reagent)

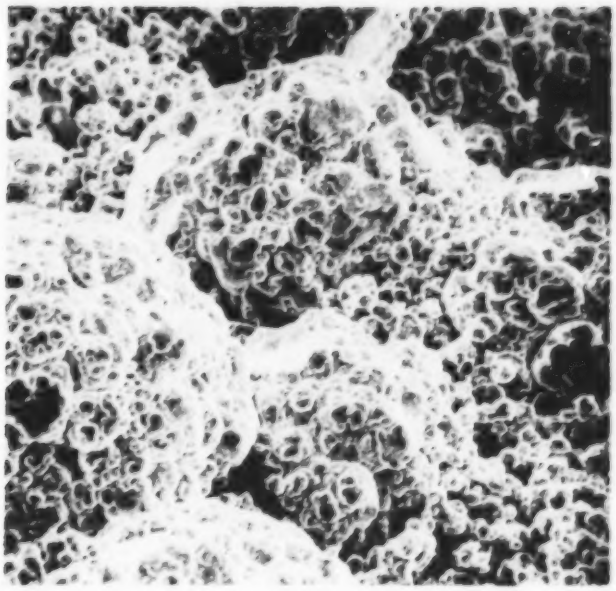

X540

Figure 14. Scanning electron micrograph of -100+140S blended with 25% G-29. Compacted at 64 ksi.

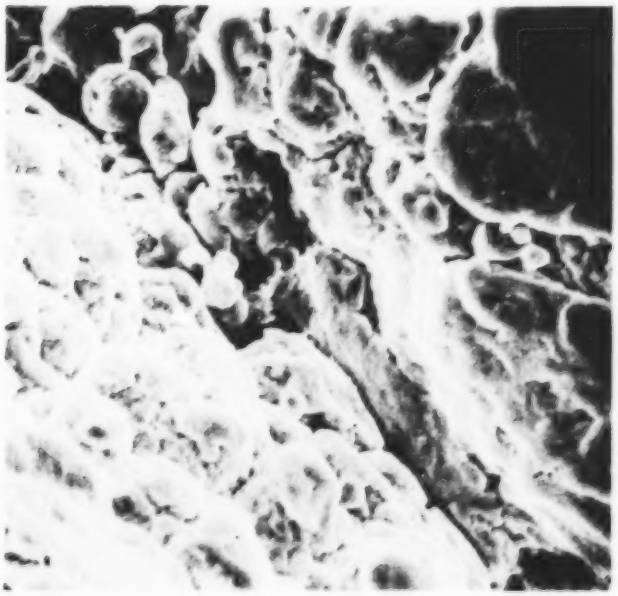

X2150

Figure 15. Same as Figure 14, at higher magnification.

X 5300

Figure 16. Same as Figures 14 and 15, at higher magnification. (Figures 14 to 16 enlarged 4.2x in printing)

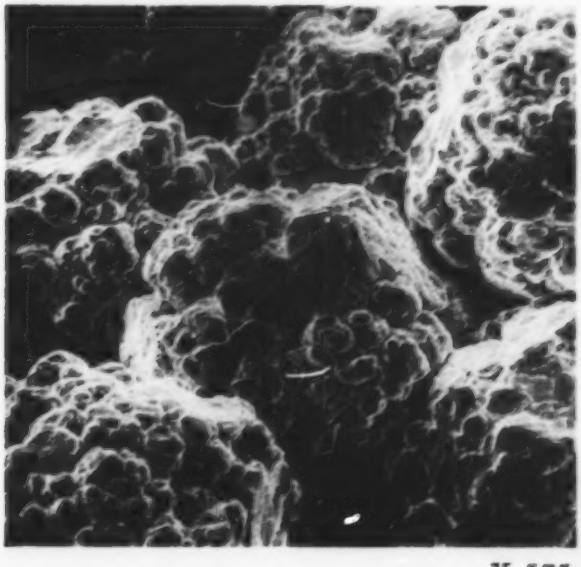

X 575

Figure 17. Scanning electron micrograph of -100+140S compacted at 96 ksi.

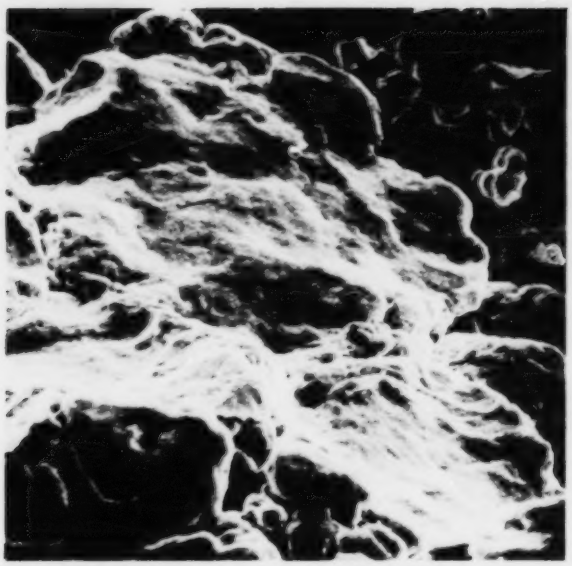

X2300

Figure 18. Same as Figure 17, at higher magnification.

(Figures 17 and 18 enlarged 3.9x in printing)